Cation Ordering in $Li[Ni_xMn_xCo_{(1-2x)}]O_2$-Layered Cathode Materials: A Nuclear Magnetic Resonance (NMR), Pair Distribution Function, X-ray Absorption Spectroscopy, and Electrochemical Study

Dongli Zeng,[†] Jordi Cabana,[†] Julien Bréger,[†] Won-Sub Yoon,[‡] and Clare P. Grey*,[†]

Department of Chemistry, State University of New York at Stony Brook, Stony Brook, New York 11794, and Brookhaven National Laboratory, Chemistry Department, Upton, New York 11973

Received August 8, 2007. Revised Manuscript Received September 7, 2007

Several members of the compositional series $Li[Ni_xMn_xCo_{(1-2x)}]O_2$ ($0.01 \leq x \leq 1/3$) were synthesized and characterized. X-ray diffraction results confirm the presence of the layered α-$NaFeO_2$-type structure, while X-ray absorption near-edge spectroscopy experiments verify the presence of Ni^{2+}, Mn^{4+}, and Co^{3+}. Their local environment and short-range ordering were investigated by using a combination of ^6Li magic angle spinning (MAS) nuclear magnetic resonance (NMR) spectroscopy and neutron pair distribution function (PDF) analysis, associated with reverse Monte Carlo (RMC) calculations. The ^6Li MAS NMR spectra of compounds with low Ni/Mn contents ($x \leq 0.10$) show several well-resolved resonances, which start to merge when the amount of Ni and Mn increases, finally forming a broad resonance at high Ni/Mn contents. Analysis of the ^6Li MAS NMR $^6Li[Ni_{0.02}Mn_{0.02}Co_{0.96}]O_2$ spectrum, is consistent with the formation of Ni^{2+} and Mn^{4+} clusters within the transition-metal layers, even at these low-doping levels. The oxidation state of Ni in this high Co content sample strongly depends upon the Li/transition metal ratio of the starting materials. Neutron PDF analysis of the highest Ni/Mn content sample $Li[Ni_{1/3}Mn_{1/3}Co_{1/3}]O_2$ shows a tendency for Ni cations to be close to Mn cations in the first coordination shell; however, the Co^{3+} ions are randomly distributed. Analysis of the intensity of the "$LiCoO_2$" resonance, arising from Li surrounded by Co^{3+} in its first two cation coordination shells, for the whole series provides further evidence for a nonrandom distribution of the transition-metal cations. The presence of the insulator-to-metal transition seen in the electrochemical profiles of these materials upon charging correlates strongly with the concentration of the "$LiCoO_2$" resonance.

Introduction

Lithium ion batteries occupy a very large portion of the portable battery market because of their high energy density and design flexibility. $LiCoO_2$ currently represents the most widely used positive electrode in most commercial rechargeable lithium batteries. It has a layered framework corresponding to the α-$NaFeO_2$ structure (space group $R\bar{3}m$, number 166) with the oxygen ions close-packed in a cubic arrangement and the transition metal (TM) and lithium ions occupying the octahedral sites in alternating layers (Figure 1). Unfortunately, the safety issues associated with $LiCoO_2$, its poor rate performance, and the toxicity of cobalt limit its use in large-scale applications. This has motivated the study of other layered compounds that contain less or no cobalt at all, such as $LiNiO_2$,[1] $LiNi_{1-y}Co_yO_2$,[2] $LiMnO_2$,[3] $LiNi_{1-y}Mn_yO_2$,[4,5]

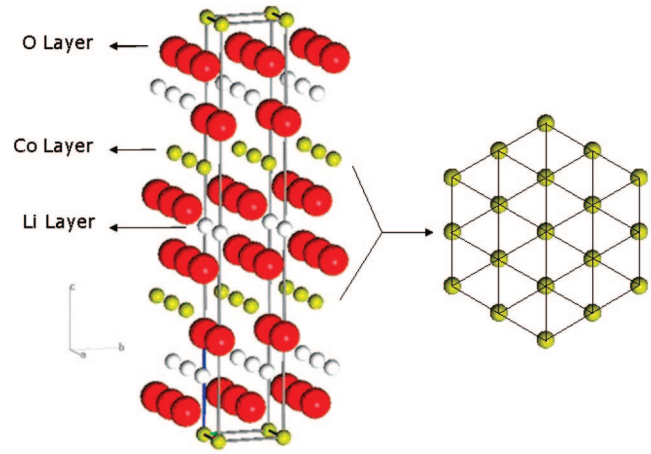

Figure 1. α-$NaFeO_2$-type structure ($R\bar{3}m$) of cathode material $LiCoO_2$. The trigonal lattice of the TM layer (Co layer here) is shown on the right.

and $LiNi_{1-y-z}Mn_yCo_zO_2$.[6,7] Among them, the members of the compositional series $Li[Ni_xMn_xCo_{(1-2x)}]O_2$, first synthesized by Ohzuku and Makimura[8] and Lu et al.,[9] show very good electrochemical behavior and, consequently, have triggered a large amount of research on these and related compounds.

* To whom correspondence should be addressed. E-mail: cgrey@notes.cc.sunysb.edu.
† State University of New York at Stony Brook.
‡ Brookhaven National Laboratory.

(1) Dahn, J. R.; von Sacken, U.; Michal, C. A. *Solid State Ionics* **1990**, *44*, 87.
(2) Saadoune, I.; Delmas, C. *J. Mater. Chem.* **1996**, *6*, 193.
(3) Capitaine, F.; Gravereau, P.; Delmas, C. *Solid State Ionics* **1996**, *89*, 197–202.
(4) Rossen, E.; Jones, C. D. W.; Dahn, J. R. *Solid State Ionics* **1992**, *57*, 311.
(5) Ohzuku, T.; Makimura, Y. *Chem. Lett.* **2001**, *744*, 745.
(6) Liu, Z.; Yu, A.; Lee, J. Y. *J. Power Sources* **1999**, *81–82*, 416–419.
(7) Yoshio, M.; Noguchi, H.; Itoh, J.-i.; Okada, M.; Mouri, T. *J. Power Sources* **2000**, *90*, 176–181.

10.1021/cm702241a CCC: $37.00
Published on Web 11/15/2007

In particular, $Li[Ni_{1/3}Mn_{1/3}Co_{1/3}]O_2$ shows a stable capacity of around 150 mA h/g in the voltage window of 3.5–4.2 V and a capacity of over 200 mA h/g upon cycling to 5.0 V.[8] First-principle calculations, backed by experimental X-ray absorption spectroscopy (XAS) results, demonstrated that the oxidation states of Ni, Mn, and Co in the pristine compound are +2, +4, and +3 respectively,[10] even though both $LiMnO_2$ and $LiNiO_2$ contain trivalent transition-metal ions.[3,11] These methods, along with ^{6}Li magic angle spinning (MAS) nuclear magnetic resonance (NMR) spectroscopy, were used to probe the local environments of the different ions and the changes in the electronic structure of the compounds upon charging. On the basis of these methods and detailed electrochemical measurements,[12] Ni^{2+} was shown to oxidize at the lowest potential and represent the major charge compensation site.[10,13–15] Ni^{2+} and Ni^{3+} are thought to be present for lithium contents (x) in $Li_x[Ni_{1/3}Mn_{1/3}Co_{1/3}]O_2$ of $^2/_3 \leq x \leq 1$, and Ni^{3+} and Ni^{4+} are thought to be present for lithium contents (x) in $Li_x[Ni_{1/3}Mn_{1/3}Co_{1/3}]O_2$ of $^1/_3 \leq x \leq ^2/_3$. Co^{3+} is oxidized to Co^{4+} for $0 \leq x \leq ^1/_3$, in the 4.88–5.2 V range, with the oxidation state of Mn^{4+} remaining unchanged through the charging process.

Despite the considerable amount of work devoted, to date, to the $Li[Ni_xMn_xCo_{(1-2x)}]O_2$ system, it still remains unclear as to how Ni/Mn ordering is disrupted by Co^{3+} doping, how the ordering and oxidation state of the three cations change across the series and as a function of the processing conditions, and most importantly, how this affects the electrochemical performance. For the related system, $Li[Li_{(1-2x)/3}Ni_xMn_{(2-x)/3}]O_2$, both first-principle calculations and experimental data from techniques that probe the local structure have provided clear evidence for strong interactions between Ni^{2+} and Mn^{4+} ions.[16] These ions tend to be next to each other in the TM layers in $Li[Ni_{0.5}Mn_{0.5}]O_2$ ($x = 0.5$ in both systems), resulting in a nonrandom distribution of cations.[17] Furthermore, in the "ideal" layered material, with limited Li/Ni exchange between the layers, the Ni and Mn ions show a tendency to order in zigzags, as opposed to chains.[18] In the case of $Li[Ni_{1/3}Mn_{1/3}Co_{1/3}]O_2$, recent ^{6}Li MAS NMR results from Cahill and co-workers are consistent with a nonrandom distribution of cations in the TM layers[19] and the authors propose a model, whereby the TM ions order to maintain a local charge balance. However, their analysis only considered the (Fermi contact) interactions between Li and its first coordination shell of TM ions. The interactions involving the second coordination shell were ignored, although these interactions can be quite large.[20,21] Nonetheless, their NMR data and analysis do provide compelling evidence for local TM clustering.

The nature of the cation ordering will also be linked to the oxidation states of the Ni and Mn ions in the $Li[Ni_xMn_xCo_{(1-2x)}]O_2$ series. Two extreme scenarios can be envisaged as x decreases and the Co^{3+} concentration increases. In the first scenario, Ni/Mn clustering is assumed. Here, the pair of cations (Ni^{2+} and Mn^{4+}) is likely to be more stable than (Ni^{3+} and Mn^{3+}). In the second case, a random distribution of the three ions on the α-$NaFeO_2$ trigonal lattice (Figure 1) is assumed. Now, as the average Ni^{2+}–Mn^{4+} separation increases, the energy penalty associated with charge separation, i.e., the cost to convert (Ni^{3+} and Mn^{3+}) to (Ni^{2+} and Mn^{4+}), increases and, in the limit of infinite dilution, the oxidation state of these two cations is likely 3+. The most likely scenario will depend upon the balance between entropic factors, which favor random distributions, and the energy penalty associated with the formation of two 3+ cations and will presumably be affected by the synthetic methods used to prepare the materials.

The work presented here uses a combination of techniques including X-ray and neutron diffraction, X-ray absorption near-edge spectroscopy (XANES), ^{6}Li MAS NMR spectroscopy, and neutron pair distribution function (PDF) analysis, along with reverse Monte Carlo (RMC) calculations, to investigate the local and long-range structure for this series of compounds. These techniques are sensitive to either the oxidation state (XANES) or the local structure surrounding the element under investigation (NMR/PDF). In particular, the cation ordering in the TM layers for the compounds with $x = 0.02$ and $^1/_3$ were studied intensively. The effect of the synthesis conditions and slight deviations of the stoichiometry are also discussed for the former material.

Experimental Section

Synthesis of the Compounds. All of the compounds prepared in the $Li[Ni_xMn_xCo_{(1-2x)}]O_2$ series ($x = 0.01$, 0.0125, 0.02, 0.025, 0.05, 0.075, 0.10, 0.125, 0.15, 0.20, 0.25, 0.30, and $^1/_3$) were synthesized following the procedure from Lu et al.,[9] using a mixed transition-metal hydroxide as a reagent to improve the mixing and the purity of the final products.[22] To prepare this hydroxide, stoichiometric amounts of $Mn(NO_3)_2 \cdot 4H_2O$ (>97.0%, Fluka), $Ni(NO_3)_2 \cdot 6H_2O$ (>98.0%, Fluka), and $Co(NO_3)_2 \cdot 6H_2O$ (98+%, Aldrich) were dissolved in 50 mL of distilled water and added dropwise into a 400 mL $LiOH \cdot H_2O$ (purified, crystal, Fisher) solution with around twice the molar amount excess to maintain a highly basic pH. The resulting precipitates, $Ni_xMn_xCo_{(1-2x)}$-

(8) Ohzuku, T.; Makimura, Y. *Chem. Lett.* **2001**, *642*, 643.
(9) Lu, Z.; MacNeil, D. D.; Dahn, J. R. *Electrochem. Solid-State Lett.* **2001**, *4* (12), A200–A203.
(10) Hwang, B. J.; Tsai, Y. W.; Carlier, D.; Ceder, G. *Chem. Mater.* **2003**, *15*, 3676–3682.
(11) Rougier, A.; Delmas, C. *Solid State Commun.* **1995**, *94* (2), 123–127.
(12) MacNeil, D. D.; Lu, Z.; Dahn, J. R. *J. Electrochem. Soc.* **2002**, *149* (10), A1332–A1336.
(13) Shaju, K. M.; Rao, G. V. S.; Chowdari, B. V. R. *Electrochim. Acta* **2002**, *48*, 145–151.
(14) Yoon, W.-S.; Grey, C. P.; Balasubramanian, M.; Yang, X.-Q.; Fischer, D. A.; McBreen, J. *Electrochem. Solid-State Lett.* **2004**, *7* (3), A53–A55.
(15) Yoon, W.-S.; Balasubramanian, M.; Chung, K. Y.; Yang, X.-Q.; McBreen, J.; Grey, C. P.; Fischer, D. A. *J. Am. Chem. Soc.* **2005**, *127*, 17479–17487.
(16) Yoon, W.-S.; Iannopollo, S.; Grey, C. P.; Carlier, D.; Gorman, J.; Reed, J.; Ceder, G. *Electrochem. Solid-State Lett.* **2004**, *7* (7), A167–A171.
(17) Bréger, J.; Dupré, N.; Chupas, P. J.; Lee, P. L.; Proffen, T.; Parise, J. B.; Grey, C. P. *J. Am. Chem. Soc.* **2005**, *127*, 7529–7537.
(18) Bréger, J.; Kang, K.; Cabana, J.; Ceder, G.; Grey, C. P. *J. Mater. Chem.* **2007**, *17*, 3167–3174.
(19) Cahill, L. S.; Yin, S.-C.; Samoson, A.; Heinmaa, I.; Nazar, L. F.; Goward, G. R. *Chem. Mater.* **2005**, *17*, 6560–6566.
(20) Carlier, D.; Ménétrier, M.; Grey, C. P.; Delmas, C.; Ceder, G. *Phys. Rev. B: Condens. Matter Mater. Phys.* **2003**, *67*, 174103.
(21) Grey, C. P.; Dupré, N. *Chem. Rev.* **2004**, *104*, 4493–4512.
(22) Jouanneau, S.; Dahn, J. R. *Chem. Mater.* **2003**, *15*, 495–499.

$(OH)_2 \cdot nH_2O$, were filtered and washed thoroughly with distilled water and, then, dried overnight at 180 °C. For the natural abundance samples, the resulting powder was ground with a stoichiometric amount of $LiOH \cdot H_2O$, made into pellets, heated first at 480 °C for 3 h, reground, repelletized, and heated at 900 °C for another 3 h. Finally, the pellets were quenched with liquid nitrogen. In the case of the ^{6}Li-enriched samples ($x = 0.02$) or the ^{7}Li-enriched sample ($x = {}^1/_3$) also described in this study, either $^6LiOH \cdot H_2O$ (90–95% ^{6}Li, FW = 41.1, Cambridge Isotope Laboratories, Inc.) (referred to as $Li[Ni_{0.02}Mn_{0.02}Co_{0.96}]O_2$, "sample 1"), $^6Li_2CO_3$ (90–95% ^{6}Li, FW = 72.11, Cambridge Isotope Laboratories, Inc., "sample 2"), or $^7LiOH \cdot H_2O$ (97% ^{7}Li, FW = 42.04, Sigma-Aldrich) was used instead.

Several compounds were prepared as references for the XANES experiments. $Li[Ni_{0.2}Co_{0.8}]O_2$ was synthesized as reported[23] using stoichiometric amounts of Li_2CO_3 (99%, Fisher), NiO (99%, Aldrich), and Co_3O_4 (Aldrich) heated, in air, at 600 °C for 15 h, quenched, and reheated at 900 °C for 24 h, followed by a final quenching in liquid nitrogen. $Li_{0.9}[Ni_{0.45}Ti_{0.55}]O_2$ was prepared by ion exchange from its sodium precursor in hexanol. A full description of the synthesis procedure is reported elsewhere.[24] Li_2MnO_3 was prepared by heating, in air, stoichiometric amounts of Li_2CO_3 and Mn_2O_3 at 650 °C for 12 h, following by quenching, and reheating at 850 °C for 24 h, with a final slow cooling in air.[25] The other reference compounds used in the study, commercial NiO (99%, Aldrich) and Mn_2O_3 (99%, Aldrich), were used without further purification.

X-ray Diffraction (XRD). XRD was carried out on a Rigaku Miniflex powder diffractometer. The 2θ range used for data collection was from 20° to 120° (chromium tube with CrK_α: λ = 2.2909 Å). A step scan of $2\theta = 0.02°$/step size was used for all samples, and the scan speed was 1°/min. Cell parameter refinements were performed using JADE XRD pattern processing 6.5 (Materials Data, Inc.).

Solid-State NMR. The ^{6}Li MAS NMR experiments were performed at 29.39 MHz on a Chemagnetics CMX-200 spectrometer ($B_0 = 4.7$ T) using a double-resonance 1.8 mm probe. Silicon nitride (Si_3N_4) rotors were used and spun at a speed of 38 kHz. All of the spectra were acquired following a rotor-synchronized Hahn echo sequence (90°-τ−180°-τ acquisition). The spectra were referenced to a standard 1 M ^{6}LiCl solution at 0 ppm. $\pi/2$ pulses of 3.5 μs were used, with a delay time of 0.2 s. A pulse-delay array was performed for the sample $Li[Ni_{0.02}Mn_{0.02}Co_{0.96}]O_2$, and fully relaxed, quantitative spectra could be obtained with a pulse delay of 0.2 s, presumably because of the presence of the paramagnetic ions in the sample.

X-ray Absorption Near-Edge Spectroscopy (XANES). The XANES spectra were collected on beamline X19A at the National Synchrotron Light Source (NSLS) at Brookhaven National Laboratory. The measurements were performed in transmission or fluorescence mode using a Si (111) double-crystal monochromator detuned to 35–45% of its original intensity to eliminate the high-order harmonics. Energy calibration was carried out by using the first inflection points in the spectri of Mn, Co and Ni metal foil as references (Mn K-edge = 6539 eV, Co K-edge = 7709 eV, and Ni K-edge = 8333 eV).

Neutron Diffraction (ND) and Pair Distribution Function (PDF) Analysis. ND experiments were performed on the General Purpose Powder Diffractometer (GPPD) at the Intense Pulsed Neutron Source (IPNS, Argonne National Laboratory, Argonne, IL) for $^7Li[Ni_{1/3}Mn_{1/3}Co_{1/3}]O_2$. The sample (around 500 mg) was packed into a ${}^1/_4$ in. inside diameter thin-walled vanadium can. The exposure time was around 12 h. The data was corrected for instrument background, sample and background absorption, and multiple scattering. Data up to $Q_{max} = 25$ Å^{-1} were used in the Fourier transform. Rietveld[26] refinement of the structure was performed with GSAS-EXPGUI,[27,28] with this neutron diffraction data. The PDF data obtained from this neutron experiment was processed using PDFgetN.[29]

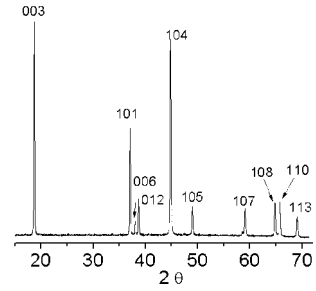

Figure 2. XRD pattern of $Li[Ni_{0.15}Mn_{0.15}Co_{0.70}]O_2$ and Miller indices corresponding to a unit cell with $R\bar{3}m$ space group. The 2θ values correspond to copper radiation ($K_{\alpha 1}$: λ = 1.5406 Å).

Electrochemistry. Cathodes were prepared by mixing 80 wt % of the active material, 10 wt % of acetylene black, and 10 wt % of polyvinylidene fluoride (PVDF) binder in *N*-methyl pyrrolidone (NMP). The slurry was deposited on an aluminum foil and dried at 80 °C until the solvent had evaporated completely. Coin cells (CR2032, Hohsen Corp.) were assembled in an argon-filled glovebox. Each cell contains typically about 15 mg of active material, separated from a Li disk by two pieces of Celgard separator (Celgard, Inc., Charlotte, NC). A 1 M solution of $LiPF_6$ in ethylene carbonate/dimethyl carbonate (1:1) was used as the electrolyte. Electrochemical experiments were carried out on a battery cycler (Arbin Instruments, College Station, TX) in galvanostatic mode at a C/50 rate.

Results and Discussion

X-ray Diffraction. The XRD patterns of $Li[Ni_xMn_xCo_{(1-2x)}]O_2$ with different values of x show similar features and are consistent with a single phase with a α-$NaFeO_2$ structure. A representative pattern for the $x = 0.15$ sample is shown in Figure 2. The clearly resolved 006/012 and 108/110 pairs of reflections indicate a well-developed layered structure.[30] Refinements using these data show an increase of the cell parameters c and a, with increasing x. This is due to the increasing amount of Ni^{2+}, which is larger than Co^{3+} [$r(Ni^{2+})$ = 0.69 Å compared to $r(Co^{3+})$ = 0.55 Å and $r(Mn^{4+})$ = 0.53 Å].[12] The actual refined values are listed in Table S1 in the Supporting Information, and the results are plotted in Figure S1 in the Supporting Information. These results are consistent with the previous study by MacNeil et al.[12]

X-ray Absorption Near-Edge Spectroscopy. Figure 3a shows selected normalized Ni K-edge XANES spectra of

(23) Saadoune, I.; Ménétrier, M.; Delmas, C. *J. Mater. Chem.* **1997**, *7*, 2505–2511.
(24) Kang, K.; Carlier, D.; Reed, J.; Arroyo, E. M.; Ceder, G.; Croguennec, L.; Delmas, C. *Chem. Mater.* **2003**, *15*, 4503–4507.
(25) Bréger, J.; Jiang, M.; Dupré, N.; Meng, Y. S.; Shao-Horn, Y.; Ceder, G.; Grey, C. P. *J. Solid State Chem.* **2005**, *178*, 2575–2585.
(26) Rietveld, H. M. *J. Appl. Crystallogr.* **1969**, *2*, 65.
(27) Larson, A. C.; Von Dreele, R. B. *General Structure Analysis System (GSAS)*; Los Alamos National Laboratory Report LAUR 86–748, 2000.
(28) Toby, B. H. *J. Appl. Crystallogr.* **2001**, *34*, 210.
(29) Peterson, P. F.; Gutmann, M.; Proffen, T.; Billinge, S. J. L. *J. Appl. Crystallogr.* **2000**, *33*, 1192.
(30) Gummow, R. J.; Thackeray, M. M.; David, W. I. F.; Hull, S. *Mater. Res. Bull.* **1992**, *27*, 327–337.

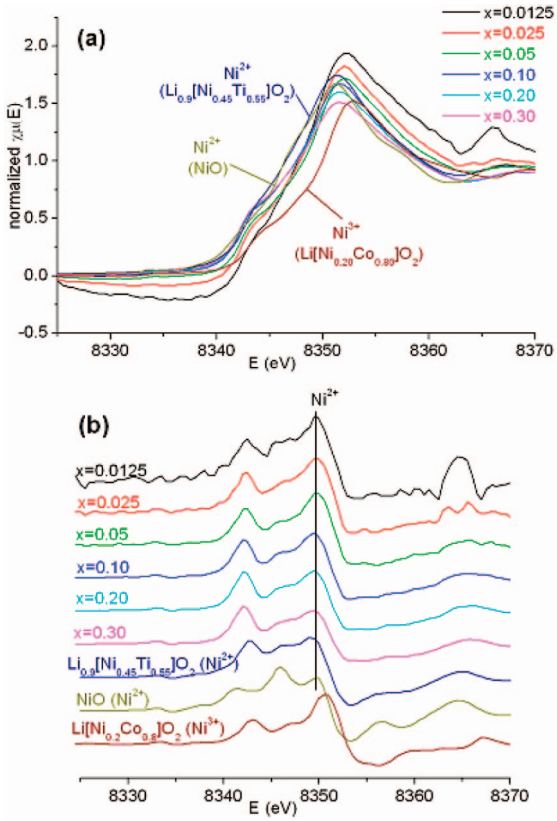

Figure 3. (a) Normalized Ni K-edge XANES spectra of selected compounds in the $Li[Ni_xMn_xCo_{(1-2x)}]O_2$ series at room temperature. Other Ni^{2+} and Ni^{3+} compounds are also included as references. (b) First derivative of the normalized Ni K-edge XANES spectra shown in a.

the $Li[Ni_xMn_xCo_{(1-2x)}]O_2$ series with different x values. Those of the reference compounds with either Ni^{2+} (NiO and $Li_{0.9}[Ni_{0.45}Ti_{0.55}]O_2$) or Ni^{3+} ($Li[Ni_{0.2}Co_{0.8}]O_2$) are also included. All of the $Li[Ni_xMn_xCo_{(1-2x)}]O_2$ compounds, even with very low x (e.g., $x = 0.0125$ and 0.025), have very similar absorption edge energy positions, close to those of NiO and $Li_{0.9}[Ni_{0.45}Ti_{0.55}]O_2$ and noticeably shifted away from that of layered $Li[Ni_{0.20}Co_{0.80}]O_2$, suggesting the existence of Ni^{2+} in our samples. This can be more clearly seen in the first derivative of the spectra (Figure 3b), where the peaks corresponding to the Ni absorption edge for our samples and the Ni^{2+} reference compounds are at the same position and at a lower energy than that for Ni^{3+} in $Li[Ni_{0.20}Co_{0.80}]O_2$.

Figures 4 and 5 correspond to the normalized Mn and Co K-edge XANES spectra, respectively. The energy of the absorption edge of the former is the same for all of the studied compounds and exhibits a clear Mn^{4+} character as in Li_2MnO_3. For Co, the energy of the absorption edge for the studied compounds is the same as that of the reference compound $Li[Ni_{0.20}Co_{0.80}]O_2$, indicating the presence of Co^{3+}.

A previous study of $Li[Ni_{1/3}Mn_{1/3}Co_{1/3}]O_2$ shows that the oxidation states for Ni, Mn, and Co are +2, +4, and +3, respectively.[14] The results presented here indicate that the compounds in the $Li[Ni_xMn_xCo_{(1-2x)}]O_2$ series ($0.01 \leq x \leq 0.30$) also consist of divalent Ni ions (Ni^{2+}), tetravalent Mn ions (Mn^{4+}), and trivalent Co ions (Co^{3+}) throughout the whole range.

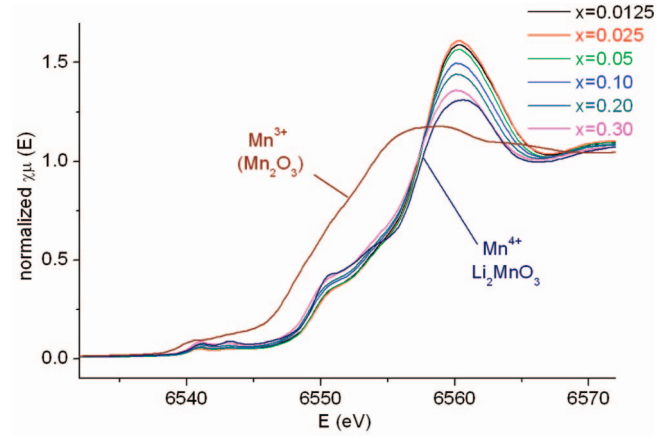

Figure 4. Normalized Mn K-edge XANES spectra of selected compounds in the $Li[Ni_xMn_xCo_{(1-2x)}]O_2$ series at room temperature, together with the Mn^{3+} and Mn^{4+} reference compounds.

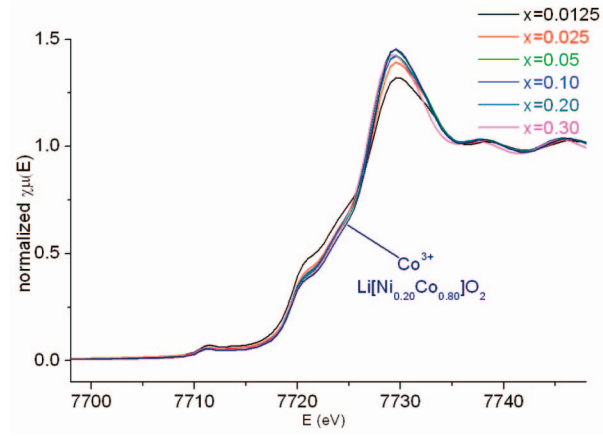

Figure 5. Normalized Co K-edge XANES spectra of selected compounds in the $Li[Ni_xMn_xCo_{(1-2x)}]O_2$ series at room temperature, together with $Li[Ni_{0.20}Co_{0.80}]O_2$, a Co^{3+} reference compound.

^{6}Li MAS NMR. *Evolution of the ^{6}Li MAS NMR Spectra along the $Li[Ni_xMn_xCo_{(1-2x)}]O_2$ Series.* Figure 6 shows the ^{6}Li MAS NMR spectra of the natural abundance $Li[Ni_xMn_xCo_{(1-2x)}]O_2$ samples, with x varying from 0.01 to $^1/_3$. Each spectrum is normalized with respect to the sample mass and the number of spectral acquisitions. The spectrum of the sample with $x = 0.01$ is dominated by a sharp 0 ppm peak, but the spectra evolve noticeably as x increases. As x varies from 0.01 to 0.10, the spectra show three major differences. The first change is a decrease of the intensity of the 0 ppm resonance as the Ni/Mn amount in the compound increases. This corresponds to a decreasing presence of a $LiCoO_2$-like local environment, in which lithium is surrounded by six Co^{3+} ions in both its first and second coordination shells. The second and third changes occur in the positive- and negative-shift regions, where several resonances (at 390, 250, 140, and −55 ppm, among others) start to appear and become more evident. However, no significant change in the shift of these signals is observed with increasing x. The local environments that give rise to these resonances will be discussed in detail later. In the samples with higher x, i.e., with even higher amounts of Ni/Mn, the well-resolved resonances observed in the compounds with low Ni/Mn contents start to merge and form a broad

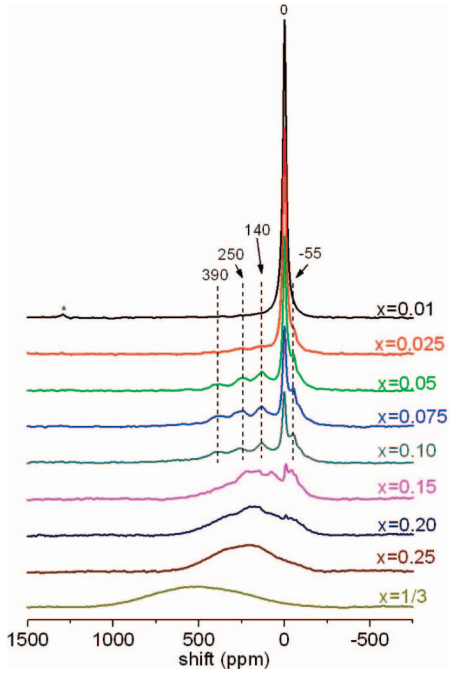

Figure 6. Evolution of the ^{6}Li MAS NMR spectra of the samples prepared in the Li[$Ni_xMn_xCo_{(1-2x)}$]O_2 series with a spinning speed of 38 kHz. The x values are shown and range from 0.01 to $^1/_3$. The most intense well-resolved isotropic resonances are indicated. The asterisk indicates a spinning sideband originating from the 0 ppm resonance.

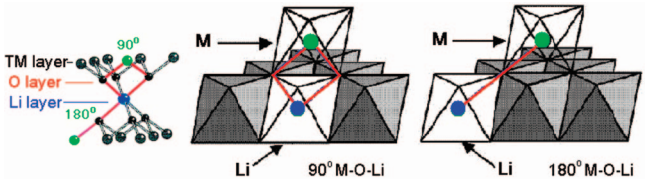

Figure 7. Graphic representation of the two possible types of interactions between the lithium ions in the lithium layer of a $LiMO_2$-type structure and the transition metal (TM = Ni, Mn, and Co, in this case) ions in the TM layer (after Carlier et al.[20]). The interactions occur via the oxygen as intermediate atoms. A representation of the geometric environment of lithium is also depicted.

resonance with the center of gravity at around 300 ppm. Additionally, the intensity of the resonance at 0 ppm significantly decreases and is ultimately buried under the broad resonance when x reaches 0.25. As a result of this, the center of gravity of the spectrum shifts to higher shift values (around 440 ppm).

To investigate the chemical environment that leads to each resonance in further detail, the ^{6}Li MAS NMR spectrum of enriched ^{6}Li[$Ni_{0.02}Mn_{0.02}Co_{0.96}$]$O_2$ (x = 0.02) was acquired and studied more extensively.

^{6}Li[$Ni_{0.02}Mn_{0.02}Co_{0.96}$]$O_2$: Implications for the Local Structure. Before the spectrum of this compound is analyzed in detail, we need to describe the possible local environments for lithium in this type of material. Each of these environments will result in a characteristic NMR signal, because of the interactions between Li and the nearby paramagnetic ions.

In the ideal layered $LiMO_2$ (M = transition metal) structure (Figure 7), each Li^+ ion has 12 neighboring transition-metal cations, 6 in the first cation coordination shell and 6 in the second cation coordination shell. There are two types of interactions between lithium ions and the unpaired electrons on the transition metals: one due to a 90° M–O–Li angle (between lithium and a TM in its first cation coordination shell), leading to a so-called 90° M–O–Li interaction and one with a 180° M–O–Li angle (between lithium and a TM in the second cation coordination shell of Li), leading to a 180° M–O–Li interaction. Similarly, each transition-metal cation interacts with six lithium ions in the layer below (or above).

Li/Ni exchange[14,31] may occur in $LiMO_2$-type compounds with high amounts of Ni, because of the similar ionic radius of Li^+ (0.74 Å) and Ni^{2+} (0.69 Å). However, previous XRD refinements showed that this exchange is extremely limited for this series of compounds when the Co content is higher than 85%.[12] For this reason, an ideal situation with no lithium/transition-metal exchange was assumed here.

Once the environments are defined, we need to assign a shift to each of them. Previous ^{6}Li NMR studies in other layered-type systems, such as Li_2MnO_3, Li[$Ni_xMn_{(2-x)/3}Li_{(1-2x)/3}$]$O_2$ and Li[Ti_xNi_{1-x}]O_2, have allowed us to estimate the values associated with the presence of a given transition metal in a given oxidation state in the first or second coordination shell of a central lithium. As a result, we established that the hyperfine shift induced by a single Mn^{4+} ion via two intervening oxygen atom(s) is around +250 ppm for one Mn^{4+} in the first coordination shell (i.e., two 90° Mn^{4+}–O–Li bonds) and −60 ppm for one Mn^{4+} in the second coordination shell (i.e., via one 180° Mn^{4+}–O–Li bond).[20,32] In the case of Ni^{2+}, the corresponding values are ca. −30 and +170 ppm, respectively.[33] Finally, for Ni^{3+}, we would expect a shift of ca. −15 ppm for the presence of two 90° Ni^{3+}–O–Li interactions (one Ni^{3+} in the first coordination shell) and +110 ppm for one 180° Ni^{3+}–O–Li interaction (one Ni^{3+} in the second coordination shell).[34,35] The shifts induced by Ni^{3+} have the same sign as those of Ni^{2+}, but they are smaller in magnitude.

Figure 8 shows a zoom of the ^{6}Li MAS NMR spectrum of ^{6}Li[$Ni_{0.02}Mn_{0.02}Co_{0.96}$]$O_2$ (sample 1). The deconvolution shows that there are eight major resonances: 390, 258, 140, 0, −24, −53, −77, and −135 ppm, which can be assigned to specific chemical environments labeled on the basis of the fact that all of the M–O–Li interactions are additive and consistent with the presence of Ni^{2+} and Mn^{4+}, as observed in the XANES spectra (Table 1). The resonance at 390 ppm is then assigned to Li^+, with one Mn^{4+} in its first coordination shell and one Ni^{2+} in its second coordination shell. Two environments are assigned to the resonance at 258 ppm: Li^+ with one Mn^{4+} and (i) zero or (ii) one Ni^{2+} in its first coordination shell. The calculated hyperfine shifts for these two environments differ by only 24 ppm and are, most likely, not resolvable. The −77 ppm resonance is assigned to Li^+ with one Ni^{2+} in the first coordination shell and one Mn^{4+}

(31) Yoon, W.-S.; Paik, Y.; Yang, X.-Q.; Balasubramanian, M.; McBreen, J.; Grey, C. P. *Electrochem. Solid-State Lett.* **2002**, *5* (11), A263–A266.
(32) Pan, C.; Lee, Y. J.; Ammundsen, B.; Grey, C. P. *Chem. Mater.* **2002**, *14*, 2289–2299.
(33) Carlier, D.; Kang, K.; Ceder, G.; Yoon, W. S.; Grey, C. P. 203rd Meeting of the Electrochemical Society (ECS), Paris, France, April 27–May 2, 2003.
(34) Marichal, C.; Hirschinger, J.; Granger, P. *Inorg. Chem.* **1995**, *34*, 1773–1778.
(35) Chazel, C.; Ménétrier, M.; Croguennec, L.; Delmas, C. *Magn. Reson. Chem.* **2005**, *43*, 849–857.

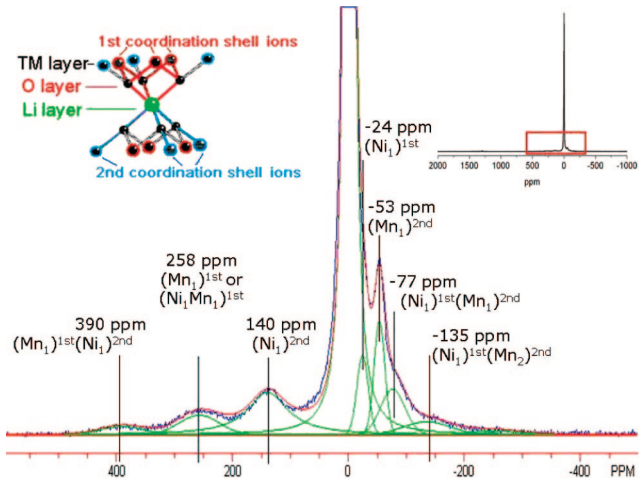

Figure 8. Zoom of the ^{6}Li MAS NMR spectrum of $^6Li[Ni_{0.02}Mn_{0.02}Co_{0.96}]O_2$ (sample 1) acquired at 38 kHz, with its corresponding deconvolution [green peaks and red line (sum)] and proposed signal assignments. (Upper right corner inset) Full spectrum; red rectangular box indicates the zoomed region. (Upper left corner inset) Arrangement of the 12 neighboring atoms around a central lithium. $(Ni_{x1}Mn_{y1})^{1st}(Ni_{x2}Mn_{y2})^{2nd}$ represents the composition of the two coordination shells for each lithium, where x and y, along with the subscripts 1 (for the first coordination shell) and 2 (for the second coordination shell), indicate the Ni^{2+} and Mn^{4+} contents, respectively. The other neighboring cations are all Co^{3+} and are omitted for clarity.

in the second coordination shell (sum of −24 and −53 ppm). The weak resonance at −135 ppm is assigned to a Li^+ located in an environment with one Ni^{2+} in its first coordination shell and two Mn^{4+} in its second coordination shell. The shift caused by Ni^{2+} ions in the second coordination shell (140 ppm) is somewhat smaller than observed in isostructural material $Li_{0.9}[Ni_{0.45}Ti_{0.55}]O_2$ (approximately +170 ppm). The hyperfine interaction is, however, known to be very sensitive to the Li–O–M bond angle, the degree of orbital overlap (covalency), and the coordination environment of the oxygen atoms. A smaller shift is quite likely for the current Mn^{4+} (and Co^{3+}) system because the more covalent Mn^{4+} (and Co^{3+}) ions may compete more effectively for binding to the nearby oxygen atoms.

While the peak positions (shift values) provide information about the cation arrangements around the lithium ions, the intensity (peak area) will provide quantitative information concerning the number of such Li environments existing in the structure. In the situation here, with 96% occupancy of the transition-metal layers by Co, noticeable differences in the distributions of the possible local environments (and, thus, the NMR spectrum) should be seen between a random Ni/Mn distribution and a model in which Ni^{2+} and Mn^{4+} are clustered. This will be demonstrated as follows: the chemical environment (shifts) distribution prediction in these two models (random and clustered) will be determined by using the probabilities for every environment obtained via calculation or simulation. The two prediction patterns will then be compared to the real spectrum. A view of the layered structure resulting from the two possible transition-metal cation distributions considered here is shown in Figure 9.

The positions of the Ni^{2+}, Mn^{4+}, and Co^{3+} ions are independent in the random model, and the probability that they are located at a given cation position in the TM layers is 0.02, 0.02, and 0.96 respectively. To simplify the analysis, only configurations with up to two Ni or Mn in the two coordination shells are considered (accounting for more than 99% of all of the possible local environments, as seen in Table 1). These possible configurations and their corresponding chemical shifts and probabilities are listed in Table 1. The normalized area of each peak in the spectra of two samples (samples 1 and 2) from different batches of $^6Li[Ni_{0.02}Mn_{0.02}Co_{0.96}]O_2$, prepared to examine the variations between samples with the same nominal compositions, are listed in the table as well.

The probability calculation for the cluster model is not as straightforward, and hence, a simulation method is used (Figure 9b). In a unit cell with 50 lithium ions, the simplest situation with one Ni^{2+} and Mn^{4+} next to each other (i.e., clustered) in the same transition-metal layer is considered. This Ni^{2+}/Mn^{4+} pair generates 7 more possible chemical environments apart from the Co-only one, and 9 (out of 50) lithium ions fall into this region. The population of lithium in each chemical environment can be easily deduced by counting them. This model has oversimplified the real situation by ignoring the possibility that there may be another Ni^{2+}/Mn^{4+} pair in the layer below and that more extended clusters may be present. This would affect some (if not all) of the 9 lithium ions that are already affected by the Ni^{2+}/Mn^{4+} pair. However, this representation depicts the most likely cluster for very dilute systems and results in noticeable differences in the populations of the different Li ions in comparison to the random model, and this should already allow us to monitor the presence of ordering in the compound.

The experimental and calculated intensities for each local environment are plotted as a function of the corresponding hyperfine shift in a histogram, for the random (Figure 10a) and cluster (Figure 10b) models. On the basis of these calculations, the structure with a random $Ni^{2+}/Mn^{4+}/Co^{3+}$ distribution is expected to have a relatively strong resonance at 0 ppm along with four weak peaks with comparable intensities at approximately +258, +140, −24, and −53 ppm. With the "cluster" constraint, the NMR spectrum is predicted to have a more intense 0 ppm peak, two weaker peaks at around +140 and −53 ppm, and three even weaker but still observable peaks at −77, +390, and +258 ppm. When the experimental data and the two models are compared, it is clear that the cluster model provides a better fit to the experimental data, with the fit being particularly good for sample 2.

Some peaks in the experimental spectrum, such as at that at +140 ppm, have slightly higher intensities than predicted with the cluster model, and there are also additional resonances because of local environments not generated with this cluster. Some of these differences arise from difficulties in resolving the different local environments. For example, the resonance from configuration 8, $Li(Ni_1Mn_1Co_4)^{1st}$, most likely is contained within the resonance ascribed to configuration 3, $Li(Mn_1Co_5)^{1st}$. The resonance at −135 ppm has to arise from three paramagnetic ions in close proximity [the lithium local environment $Li(Ni_1Co_5)^{1st}(Mn_2Co_4)^{2nd}$]. The Mn–Ni–Mn cluster, where the three cations are in a linear

Table 1. Summary of the Probabilities Resulting from the Two Models Described in the Text and Normalized Peak Areas Resulting from the Deconvolution of the Experimental Spectra for the Two Samples of $^6Li[Ni_{0.02}Mn_{0.02}Co_{0.96}]O_2$

			model				spectra deconvolution	
			random		clustered			
index number	configuration	shift (ppm)	calculation	P_{random}	calculation	$P_{cluster}$	sample 1 normalized area	sample 2 normalized area
1	$(Co_6)^{1st}(Co_6)^{2nd}$	0	1×0.96^{12}	0.613	(50–9)/50	0.82	0.7605[a]	0.8236[a]
2	$(Ni_1Co_5)^{1st}(Co_6)^{2nd}$	−24	$6 \times 0.02 \times 0.96^{11}$	0.077	1/50	0.02	0.0309	0.0225
3	$(Mn_1Co_5)^{1st}(Co_6)^{2nd}$	+258	$6 \times 0.02 \times 0.96^{11}$	0.077	1/50	0.02	0.0269	0.0233
4	$(Co_6)^{1st}(Ni_1Co_5)^{2nd}$	+140	$6 \times 0.02 \times 0.96^{11}$	0.077	2/50	0.04	0.0607	0.0533
5	$(Co_6)^{1st}(Mn_1Co_5)^{2nd}$	−53	$6 \times 0.02 \times 0.96^{11}$	0.077	2/50	0.04	0.0424	0.0281
6	$(Ni_1Co_5)^{1st}(Mn_1Co_5)^{2nd}$	−77	$6 \times 6 \times 0.02^2 \times 0.96^{10}$	0.009	1/50	0.02	0.0379	0.0298
7	$(Mn_1Co_5)^{1st}(Ni_1Co_5)^{2nd}$	+398	$6 \times 6 \times 0.02^2 \times 0.96^{10}$	0.009	1/50	0.02	0.0125	0.0078
8	$(Ni_1Mn_1Co_4)^{1st}(Co_6)^{2nd}$	+234	$6 \times 5 \times 0.02^2 \times 0.96^{10}$	0.009	1/50	0.02		
9	$(Co_6)^{1st}(Ni_1Mn_1Co_4)^{2nd}$	+87	$6 \times 5 \times 0.02^2 \times 0.96^{10}$	0.009				
10	$(Ni_1Co_5)^{1st}(Ni_1Co_5)^{2nd}$	+116	$6 \times 6 \times 0.02^2 \times 0.96^{10}$	0.009				
11	$(Mn_1Co_5)^{1st}(Mn_1Co_5)^{2nd}$	+205	$6 \times 6 \times 0.02^2 \times 0.96^{10}$	0.009				
12	$(Ni_2Co_4)^{1st}(Co_6)^{2nd}$	−48	$1/2 \times 6 \times 5 \times 0.02^2 \times 0.96^{10}$	0.004				
13	$(Mn_2Co_4)^{1st}(Co_6)^{2nd}$	+516	$1/2 \times 6 \times 5 \times 0.02^2 \times 0.96^{10}$	0.004				
14	$(Co_6)^{1st}(Ni_2Co_4)^{2nd}$	+280	$1/2 \times 6 \times 5 \times 0.02^2 \times 0.96^{10}$	0.004				
15	$(Co_6)^{1st}(Mn_2Co_4)^{2nd}$	−106	$1/2 \times 6 \times 5 \times 0.02^2 \times 0.96^{10}$	0.004				
16	$(Ni_1Co_5)^{1st}(Mn_2Co_4)^{2nd}$	−135					0.0209	0.0104
17		−250					0.0072	0.0015
			total	0.991		1	1	1

[a] The area of spinning sidebands has been included in the intensity of the 0 ppm peak.

chain, in the same layer, will give rise to this new local environment, in addition to local environments already described in Table 1, suggesting that this resonance is a signature for more extended clustering. The three cations could also be in two different layers. The resonance at −250 ppm must also be associated with extended clustering and is consistent with an environment with three Ni^{2+} and three Mn^{4+} in the first and second Li^+ cation coordination shells, respectively. Again, although the cations can be in more than one layer, this environment also arises from the extended cluster formed from a triangle of three adjacent Ni^{2+} ions, capped by three adjacent Mn^{4+} to form a larger triangle. Sample 1 appears to contain more extended clustering. It also contains a weaker 0 ppm resonance, suggesting that there are also regions or domains in the sample containing less clustering.

Investigation of the Effect of the Doping Level on the Local Structure. As seen in Figure 6, the intensity of the 0 ppm peak, which is correlated with the amount of Li^+ in a $LiCoO_2$-like local environment, decreases as the doping level of Ni/Mn in the compound increases. The normalized experimental 0 ppm peak intensities obtained from the deconvolution of the spectra were compared to the probabilities of the $LiCoO_2$-like environment [$Li(Co_6)^{1st}(Co_6)^{2nd}$] in both the random and cluster models (Figure 11). In the random model, for a compound Li[$Ni_xMn_xCo_{(1-2x)}$]O_2 with a given x, the probability for one Co to be located in a given position in the TM layers is $(1 - 2x)$ and, thus, the probability of the $Li(Co_6)^{1st}(Co_6)^{2nd}$ environment is $(1 - 2x)^{12}$. In the cluster model, an approximation is made here to calculate the probability of the $Li(Co_6)^{1st}(Co_6)^{2nd}$ environment: instead of considering the three cations individually [Ni, Mn, and Co with concentrations x, x, and $(1 - 2x)$, respectively], only two random species, Ni/Mn pairs and Co cations, with concentrations x and $(1 - 2x)$ respectively, are considered. The probability for one Co to be located in a given position is then $(1 - 2x)/[x + (1 - 2x)]$, which simplifies to $(1 - 2x)/(1 - x)$, and the probability of the $Li(Co_6)^{1st}(Co_6)^{2nd}$ environment under this approximation is then $[(1 - 2x)/(1 - x)]^{12}$. However, because the Ni/Mn pair is the species that is considered, this approximation underestimates the total configuration numbers by excluding possible configurations, where only one cation from the Ni/Mn pair affects the Li environment (i.e., the Ni or Mn cation is in its first or second coordination shell), while the other cation of the pair is in the third coordination shell, e.g., configurations $Li(Co_6)^{1st}(Ni_1Co_5)^{2nd}$ and $Li(Co_6)^{1st}(Mn_1Co_5)^{2nd}$. Thus, the calculated probability $[(1 - 2x)/(1 - x)]^{12}$ is overestimated. Despite this, the comparison of the experimental data to the calculated probabilities in the two models clearly shows that the normalized experimental 0 ppm peak intensities are higher than the calculated probabilities in the random model. The calculated probabilities in the cluster model with the approximation are very close to the experimental data in the low Ni/Mn component samples. As the doping level of Ni/Mn increases, the concentrations predicted on the basis of the pair model are higher than those seen experimentally. This is due to the fact that more possible configurations are excluded when there are more Ni/Mn in the TM layers and is likely due to the limitations of the model. In conclusion, the data show clear evidence for a degree of clustering in these samples, consistent with the results presented above for $x = 0.02$.

Effect of the Starting Lithium Stoichiometry on the Cation Ordering in TM Layers. The effect of the initial Li/TM ratio in the starting materials used to prepare the sample with 2% Ni and 2% Mn doping on the ^6Li NMR results was explored, to determine whether this affects the cation ordering of the compound. Figure 12 shows an expansion of the ^6Li NMR spectra of three samples with stoichiometry $^6Lix_0[Ni_{0.02}Mn_{0.02}Co_{0.96}]O_2$, where $x_0 = 0.95$, 1.00, and 1.05, respectively. Although the spectra of all three samples are qualitively similar, the resonance at 140 ppm, assigned to Ni in the second coordination shell, is clearly shifted to a lower value of approximately 120 ppm in the lithium-overstoichiometric sample, $^6Li_{1.05}$-

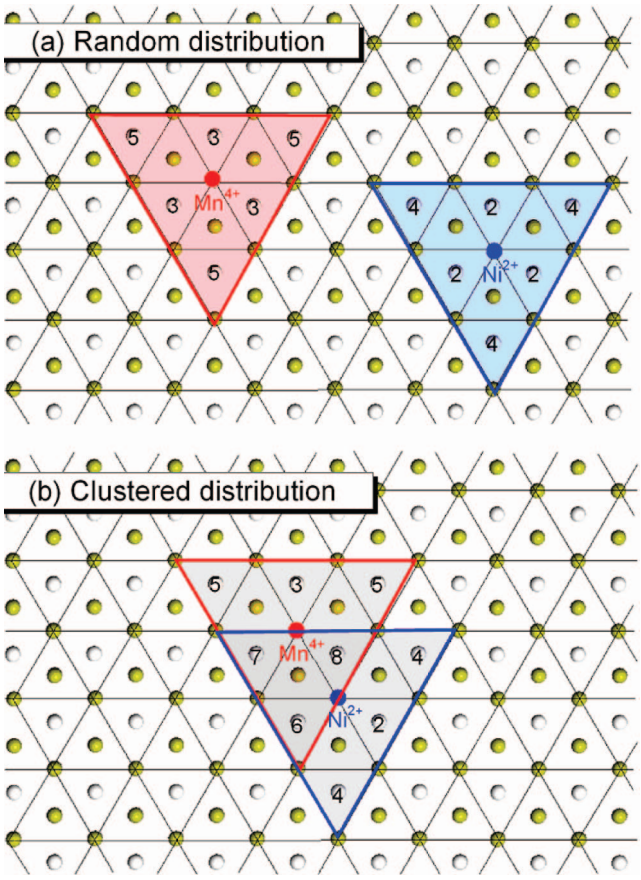

Figure 9. Graphic representation of the two possible cation distributions in a layered O3 structure. Only one of the possible distributions for the random model is shown. White balls correspond to lithium ions, and yellow balls correspond to cobalt lying in the transition-metal layers above (crossed by the solid lines of the triangular lattice) and below (in the centers of the small triangles) the lithium layer. Red and blue balls in the diagram represent Mn^{4+} and Ni^{2+}, respectively, and the red and blue large triangles indicate the region in which lithium ions interact with these ions, either through a 180° or 90° interaction, with Mn^{4+} and Ni^{2+}, respectively. Oxygen atoms are omitted for clarity. The numbers refer to the different possible configurations in each model, as shown in Table 1. When the same environment is observed in both models, the same number is used (e.g., configuration "3" refers to the local environment for lithium $(Mn_1Co_5)^{1st}(Co_6)^{2nd}$ in both models). All of the unlabeled lithium ions correspond to the $(Co_6)^{1st}(Co_6)^{2nd}$ local environment and correspond to configuration 1 in Table 1.

$[Ni_{0.02}Mn_{0.02}Co_{0.96}]O_2$. This is ascribed to the substitution of some of the excess Li^+ in the transition-metal layers and the associated oxidation of some of the Ni ions to Ni^{3+}, which is required for charge compensation. Because of the presence of some Ni^{3+}, the Ni/Mn clustering may not be as prevalent. This may result in some isolated Mn cations, which are likely present as Mn^{3+}. We tentatively assign the resonance at −43 ppm to the local environments containing this ion in the second coordination shell. Finally, no significant changes are observed for the resonances at 250 and −55 ppm, generated by the presence of Mn^{4+}, indicating that those environments remain the same for both compositions. The spectra of the stoichiometric sample, $^6Li_{1.00}[Ni_{0.02}Mn_{0.02}Co_{0.96}]O_2$, and the lithium-deficient sample, $^6Li_{0.95}[Ni_{0.02}Mn_{0.02}Co_{0.96}]O_2$, are similar, but the intensities of the resonances nearby the paramagnetic ions are weaker. In addition, the line shapes of the −55, 140, and 250 ppm resonances are slightly different. The changes are ascribed to Li^+ vacancies in the Li layers. These vacancies will also result in the formation of some Ni^{3+}, but presumably, these cations will not be detected because they are nearby Li-ion vacancies (in the Ni^{3+} second coordination shell) and not Li^+.

Neutron Scattering Studies of $^7Li[Ni_{1/3}Mn_{1/3}Co_{1/3}]O_2$. *Powder Neutron Diffraction.* Figure 13 shows the neutron diffraction pattern of $^7Li[Ni_{1/3}Mn_{1/3}Co_{1/3}]O_2$, together with the calculated and difference curves obtained by Rietveld refinement. The resulting structural parameters are shown in Table 2.

Good agreements are seen between the experimental data and patterns calculated with the $LiCoO_2$ structural model (space group $R\bar{3}m$). Close examination of the diffraction patterns revealed weaker peaks, which could not be indexed with the $R\bar{3}m$ space group. These peaks can, however, be ascribed to impurities in the material, corresponding to oxides containing Ni, Co, and/or Mn. Allowing Li/Ni exchange between the TM and Li layers of $Li[Ni_{1/3}Mn_{1/3}Co_{1/3}]O_2$ yields a small occupancy (<2%) of Ni in the Li layer. This refinement led to the following cell parameters: c = 14.2235(1) Å and a = 2.85939(1) Å. These results are consistent with a previous Rietveld refinement of the $Li[Ni_{1/3}Mn_{1/3}Co_{1/3}]O_2$ pattern from ND data, which gave c = 14.227(8) Å and a = 2.860(2) Å, with R_{wp} = 2.95%,[36] and with previous NMR data on a similar material, which indicated a 2–4% Li/Ni exchange between the Li and TM layers.[14,19]

PDF Analysis and RMC Calculations. The neutron PDF was calculated from the neutron diffraction data for $^7Li[Ni_{1/3}Mn_{1/3}Co_{1/3}]O_2$ (Figure 14). This calculation consists of a Fourier transform of all of the scattering data (both Bragg and diffuse scatterings) and is not dependent upon the model used to describe the diffraction data. The first correlation distance at around 2 Å corresponds to a superposition of the M–O distances, where M = Li, Ni, Co, and Mn. The intensity of this peak is positive, because the contribution from the positive coherent scattering lengths of Ni and Co atoms (see Table 3) are larger than those from elements with negative scattering lengths (^{7}Li and Mn). The second peak at around 2.9 Å is ascribed to the M–M and O–O bonds, where M can be Li, Ni, Mn, or Co. Peaks below 1.9 Å are termination ripples because of the cutoff of the Fourier transform at a finite Q and do not correspond to any real correlations in the structural model. All of the other peaks (above 3 Å) are a superposition of numerous environments and, therefore, are not straightforward to assign.

A fit of the experimental data using RMC calculations[37,38] was performed to explore a possible ordering of the Ni/Co/Mn atoms in $^7Li[Ni_{1/3}Mn_{1/3}Co_{1/3}]O_2$, in a similar approach to the one used for $^7Li(NiMn)_{0.5}O_2$, as previously reported.[17,18] The cell parameters determined from the Rietveld refinement of the neutron data were used in the RMC calculations, which

(36) Yin, S.-C.; Rho, Y.-H.; Swainson, I.; Nazar, L. F. *Chem. Mater.* **2006**, *18*, 1901–1910.
(37) McGreevy, R. L.; Pusztai, L. *Mol. Simul.* **1988**, *1*, 359.
(38) Tucker, M. G.; Dove, M. T.; Keen, D. A. *J. Appl. Crystallogr.* **2001**, *34*, 630.

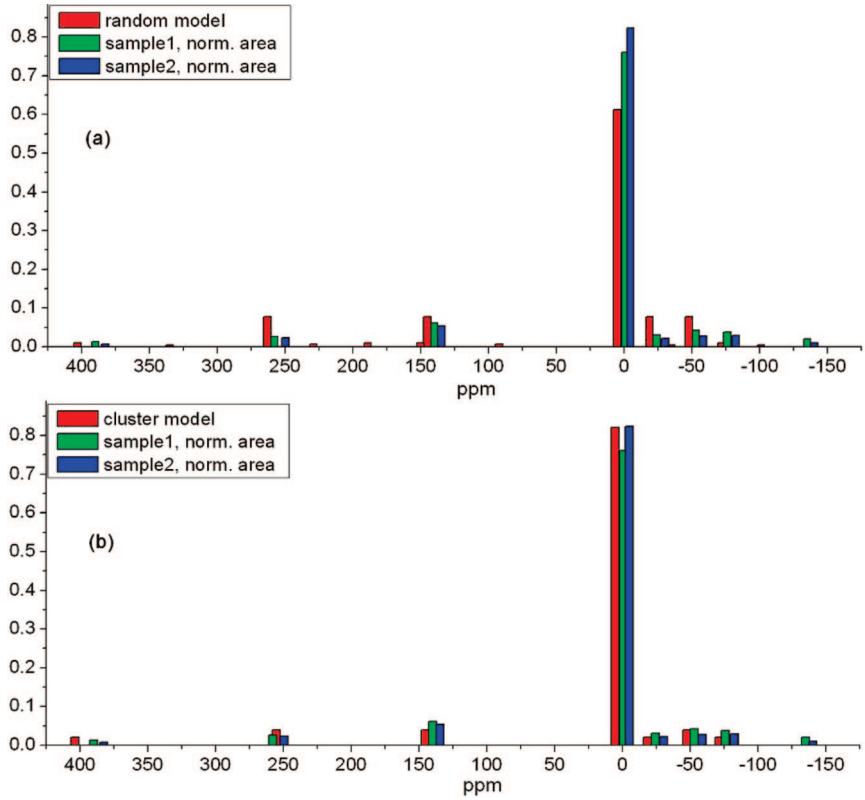

Figure 10. Comparison of the probabilities resulting from (a) the random and (b) the cluster models, with the normalized experimental peak intensities obtained from the deconvolution of the spectra of the two $^6Li[Ni_{0.02}Mn_{0.02}Co_{0.96}]O_2$ samples.

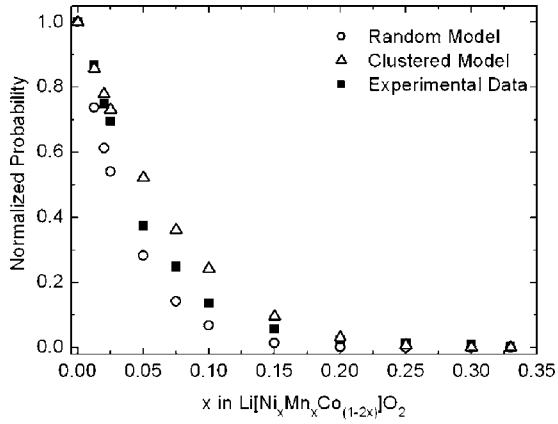

Figure 11. Comparison of the normalized 0 ppm peak intensity obtained from the deconvolution of the spectra of the Li[$Ni_xMn_xCo_{(1-2x)}$]O_2 series with the calculated probabilities in the random and clustered models.

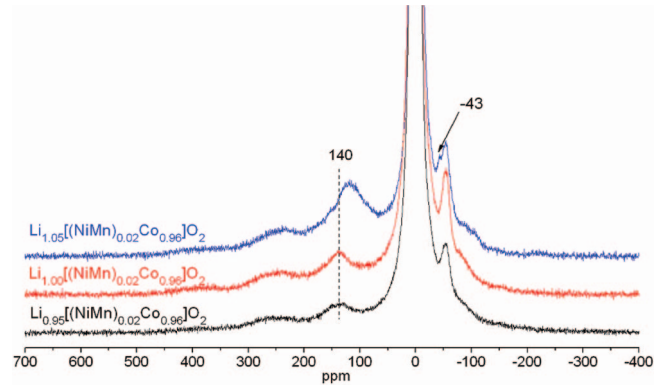

Figure 12. Expansion of the ^6Li MAS NMR spectra of $^6Li_{0.95}[Ni_{0.02}Mn_{0.02}Co_{0.96}]O_2$ (black), $^6Li_{1.00}[Ni_{0.02}Mn_{0.02}Co_{0.96}]O_2$ (red), and $^6Li_{1.05}[Ni_{0.02}Mn_{0.02}Co_{0.96}]O_2$ (blue), acquired at 38 kHz. The shifts of key resonances are indicated (see the text).

were performed with the DISCUS program.[39] Initially, a cluster comprising 10 × 10 × 2 ($a \times a \times c$) unit cells (2400 atoms) was built. Given the low amount (<2%) of Li/Ni site exchange obtained from the Rietveld refinement of the diffraction data, 0% exchange was assumed. The Ni, Co, and Mn atoms were placed in a random arrangement on the TM layers. Given their relatively small concentration, the impurities were not introduced as a second phase in the calculations. The difference between the resulting calculated PDF and the experimental data is shown in Figure 15a. The match is clearly quite poor, and thus, further structural refinement is needed. To accomplish this, RMC calculations were carried out as follows: Ni, Co, and Mn atoms were swapped randomly, and all of the atoms were allowed to relax in the *ab* plane; if a generated move improved the fit, the move was accepted. The final calculated PDF is shown in Figure 15b. A clear improvement to the fit of the experimental data over that calculated from the ideal $LiCoO_2$ model was obtained, and most of the major features appear to be captured.

The number of each different cation pair before and after the RMC calculations is reported in Table 4. The ordering of the Ni and Mn cations in the TM layers is clearly nonrandom, with Ni closer to more Mn in the first coordination shell and to more Ni in the second coordination shell than would be expected for such an arrangement, as indicated by the negative and positive Ni/Mn occupational correlations

(39) Proffen, T.; Neder, R. B. *J. Appl. Crystallogr.* **1997**, *30*, 171.

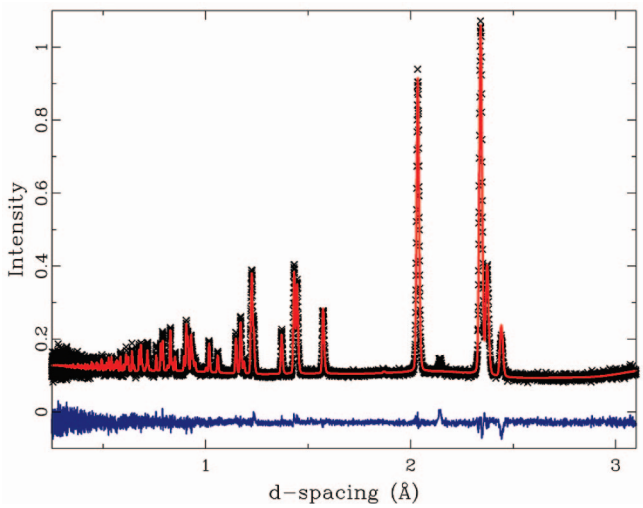

Figure 13. Results of the Rietveld refinement of $^{7}Li[Ni_{1/3}Mn_{1/3}Co_{1/3}]O_2$ using neutron diffraction data (bank 4, ±90°, of the GPPD detector). The crosses and the solid red line represent the experimental data and the calculated pattern, respectively. The difference between the calculated and experimental patterns is shown in blue, below the data. The resulting structural parameters are given in Table 2.

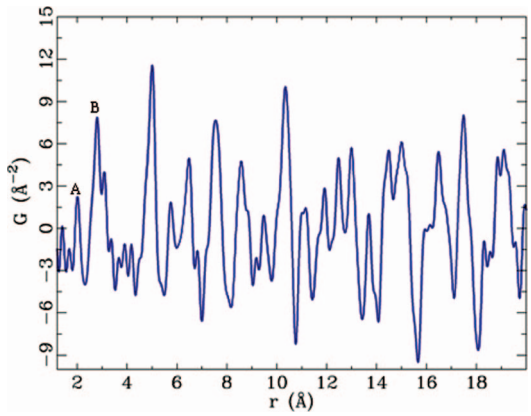

Figure 14. Pair distribution function (PDF, $G(r)$ versus distance r) for $^{7}Li[Ni_{1/3}Mn_{1/3}Co_{1/3}]O_2$. The peaks assignments are (A) M–O distances and (B) M–M and O–O distances, where M is Li, Ni, Co, or Mn.

Table 2. Structural parameters resulting from the Rietveld refinement of $^{7}Li[Ni_{1/3}Mn_{1/3}Co_{1/3}]O_2$ using neutron diffraction data. Simultaneous refinement with the same parameters of four different histograms was performed, corresponding to banks 2, 3, 4 and 5 of the GPPD detector

	$^{7}Li[Ni_{1/3}Mn_{1/3}Co_{1/3}]O_2$
space group	$R\bar{3}m$
a (Å)	2.85939(1)
c (Å)	14.2235(1)
V (Å^3)	100.713(1)
z(O)	0.24091(2)
Li/Ni exchange (%)	1.9(1)
100**Uiso* (Å^2)	
Li/Ni (3a)	3.18(4)
Ni/Co/Mn/Li (3b)	1.57(2)
O (6c)	0.500(7)
bank 2 (±125°) R_{wp} (%)	5.49
bank 3 (±107°) R_{wp} (%)	5.20
bank 4 (±90°) R_{wp} (%)	5.30
bank 5 (±53°) R_{wp} (%)	5.89

for the first and second coordination shells, respectively. In contrast, the Ni/Co and Mn/Co occupational correlations are much closer to zero, indicating a close to random distribution for these cations. Only a very slight tendency for Co to be

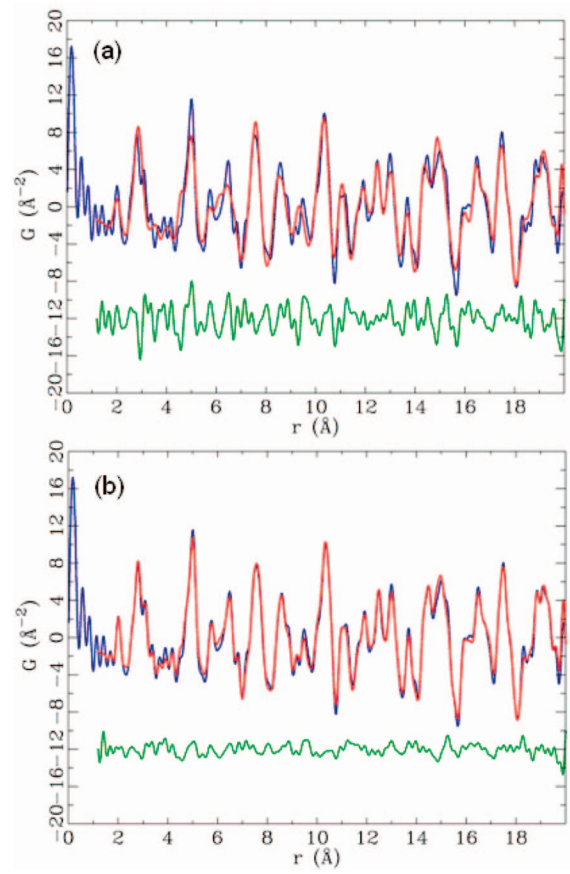

Figure 15. Fit of the experimental NPDF data for $^{7}Li[Ni_{1/3}Mn_{1/3}Co_{1/3}]O_2$ with the calculated structural model (a) before (random ordering) and (b) after the RMC calculations. The blue line represents the experimental data, and the solid red line represents the calculated PDF. The difference between the calculated and experimental patterns is shown in green.

Table 3. Coherent Neutron Scattering Lengths b_i (fm) of the Different Isotopes[45]

^{7}Li	Co	Ni	Mn	O
−2.22	2.49	10.3	−3.73	5.80

surrounded more by Ni or Mn than by Co can be observed for the first coordination shell. We note, however, that given the much smaller (positive) neutron scattering factor of Co (in comparison to Ni), the sensitivity of this method to correlations involving Co will lower, which may lead to an *underestimation* of the cation ordering, particularly that involving Co. On the basis of these results, the Ni atoms are, on average, surrounded by 1.6 Ni, 1.8 Co, and 2.5 Mn ions in the first coordination shell and by 2.8 Ni, 1.2 Co, and 2.0 Mn ions in the second coordination shell.

The results were compared to three different possible cation-ordering schemes shown in Figure 16 derived from the α-$NaFeO_2$ lattice. The first scheme (Figure 16a) is the so-called [$\sqrt{3} \times \sqrt{3}$] R30°-type superlattice,[40–42] in which all three metal cations order on a triangular lattice to maintain the 3-fold symmetry. The second ordering scheme (Figure

(40) Koyama, Y.; Yabuuchi, N.; Tanaka, I.; Adachi, H.; Ohzuku, T. *J. Electrochem. Soc.* **2004**, *151* (10), A1545–A1551.
(41) Koyama, Y.; Tanaka, I.; Adachi, H.; Makimura, Y.; Ohzuku, T. *J. Power Sources* **2003**, *119–121*, 644–648.
(42) Yabuuchi, N.; Koyama, Y.; Nakayama, N.; Ohzuku, T. *J. Electrochem. Soc.* **2005**, *152* (7), A1434–A1440.

Table 4. Number of Ni/Mn/Co Pairs in the Transition-Metal Layers (*ab* Plane) of $^7Li[Ni_{1/3}Mn_{1/3}Co_{1/3}]O_2$, Occupational Correlation Results before and after the RMC Calculations,[a] and a Comparison with the Number of Cation Pairs in the Four Models

	RMC results		possible models			
	before (random) (%)	after (%)	random (%)	[$\sqrt{3} \times \sqrt{3}$] R30° superlattice	parallel cation chains (%)	zigzag arrangement (%)
(a) First Coordination Shell						
percentage of Ni–Ni pairs	11.8 (212 pairs, p)	9.1 (164 p)	11.1	0	16.7	22.2
percentage of Ni–Mn pairs	24.4 (439 p)	28.4 (512 p)	22.2	33.3	16.7	11.1
percentage of Mn-Mn pairs	12.0 (216 p)	9.6 (172 p)	11.1	0	16.7	22.2
percentage of Ni-Co pairs	20.4 (367 p)	21.7 (390 p)	22.2	33.3	16.7	11.1
percentage of Mn-Co pairs	20.3 (365 p)	21.1 (380 p)	22.2	33.3	16.7	11.1
percentage of Co-Co pairs	11.2 (201 p)	10.1 (182 p)	11.1	0	16.7	22.2
total	100	100	100	100	100	100
correlation c_{NiMn}[b]	−0.012	−0.211				
correlation c_{NiCo}[b]	+0.067	−0.064				
correlation c_{MnCo}[b]	+0.058	−0.035				
(b) Second Coordination Shell						
percentage of Ni–Ni pairs	12.2 (220 p)	15.8 (285 p)	11.1	33.3	0	16.7
percentage of Ni–Mn pairs	21.4 (386 p)	14.1 (254 p)	22.2	0	33.3	16.7
percentage of Mn–Mn pairs	13.1 (236 p)	16.8 (302 p)	11.1	33.3	0	16.7
percentage of Ni–Co pairs	22.4 (404 p)	22.6 (406 p)	22.2	0	33.3	16.7
percentage of Mn–Co pairs	21.0 (378 p)	21.0 (378 p)	22.2	0	33.3	16.7
percentage of Co–Co pairs	9.8 (176 p)	9.7 (175 p)	11.1	33.3	0	16.7
total	100	100	100	100	100	100
correlation c_{NiMn}[b]	+0.076	+0.400				
correlation c_{NiCo}[b]	−0.018	+0.045				
correlation c_{MnCo}[b]	+0.035	+0.096				

[a] A 10 × 10 × 2 cluster size was used, and only the first and second coordination shells are considered. [b] The correlation coefficient c_{ij} between a pair of sites i and j is given by the statistical definition[46] of the correlation: $c_{ij} = (P_{ij} - \theta^2)/(\theta(1 - \theta))$, where P_{ij} is the probability that both sites i and j are occupied by the same atom type and θ is its overall occupancy. Negative values of c_{ij} indicate that the sites i and j tend to be occupied by different atom types.

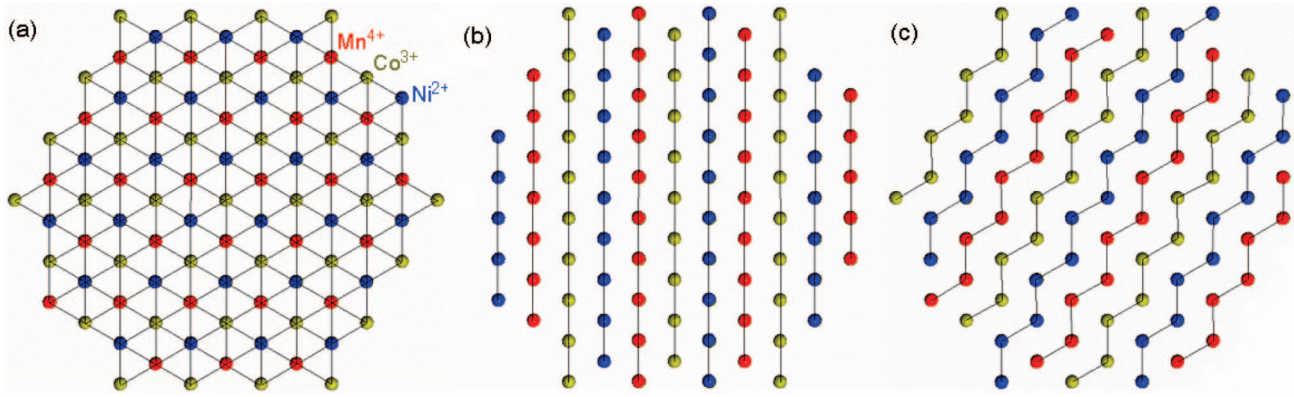

Figure 16. Schematic illustrations of the three ordered models proposed in the text for one TM layer in $Li[Ni_{1/3}Mn_{1/3}Co_{1/3}]O_2$: (a) [$\sqrt{3} \times \sqrt{3}$] 30°-type superlattice, (b) parallel, and (c) zigzag arrangements.

16b), in which the three cations order in parallel chains, was assumed in the theoretical work of Hwang et al.[10] Finally, because a zigzag arrangement of the Ni and Mn ions represents the ground state for $Li[Ni_{0.5}Mn_{0.5}]O_2$,[16] a third scheme was constructed, which comprises zigzag chains of the three cations (Figure 16c). The three ordering schemes show different correlations in the first coordination shell. Total avoidance between the same cations (0% for the Ni–Ni, Mn–Mn, and Co–Co pairs) is seen for the [$\sqrt{3} \times \sqrt{3}$] R30°-type superlattice structure. The parallel chain arrangement shows an equal concentration of all of the different pairings (16.7% for all of the pairs), while the zigzag arrangement is associated with the highest preference for clustering of like cations (22.2% for the Ni–Ni, Mn–Mn, and Co–Co pairs). For the second coordination shell (Table 4b), total avoidance between different cations (0% for Ni–Mn, Mn–Co, and Co–Ni pairs) is seen for the [$\sqrt{3} \times \sqrt{3}$] R30°-type superlattice structure, while a high preference is observed for the same cations (33.3% for Ni–Ni, Mn–Mn, and Co–Co pairs). In contrast, the parallel chain arrangement shows high preference for Ni–Mn, Mn–Co, and Co–Ni pairs (33.3%). Finally, the zigzag arrangement results in an equal amount of all of the pairs.

When the RMC calculation results are compared to the four structural models (random, [$\sqrt{3} \times \sqrt{3}$] R30°-type superlattice, parallel chain, and zigzag arrangements), the cation arrangements in the TM layers in $Li[Ni_{1/3}Mn_{1/3}Co_{1/3}]O_2$ fit two models to some degree. On one hand, the increase in the number of Ni–Mn pairs in the first coordination shell but decrease in the second coordination shell is consistent with the [$\sqrt{3} \times \sqrt{3}$] R30°-type superlattice, while the number of Ni–Co, Mn–Co, and Co–Co pairs in both shells are closer to those resulting from the random model.

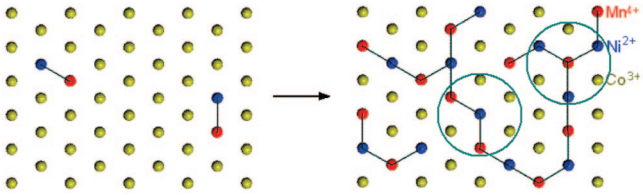

Figure 17. Schematic illustration of isolated Ni/Mn pairing at low doping levels (left) and the formation of longer chains of Ni–Mn arrangements at increased doping levels (right). Some [$\sqrt{3} \times \sqrt{3}$] superlattice motifs are illustrated with green circles.

The ^{6}Li NMR spectrum of $Li[Ni_{1/3}Mn_{1/3}Co_{1/3}]O_2$ reinforces this analysis. The absence of discrete peaks and the broad features of the resonance[14,19] are consistent with a lack of complete ordering of the cations in the TM layers, even at a local level. The tendency for [$\sqrt{3} \times \sqrt{3}$]-type ordering is consistent with the model of Cahill et al.,[19] where the local charge balance is proposed (comprising triangles of Co^{3+}, Ni^{2+}, and Mn^{4+}), and also suggests that more long-range ordering may be present in small domains in some samples, consistent with the transmission electron microscopy (TEM) data for this material.[42]

Local ordering schemes that resemble the [$\sqrt{3} \times \sqrt{3}$] superlattice presumably represent the most stable ordered configuration, because this scheme maximizes the favorable Ni–Mn contacts while minimizing high-energy Mn^{4+}–Mn^{4+} Coulombic interactions. However, the driving force for ordering involving Co^{3+} in the α-$NaFeO_2$ sublattice is much weaker because of the 3+ charge on this cation, and entropic factors will favor the disruption of the Ni–Mn ordering by Co^{3+}. Furthermore, there are no energy penalties associated with Co–Co pair formation, and the presence of these pairs (or more extended chains) will not prevent the formation of longer chains of Ni–Mn arrangements but will well prevent the long-range ordering of the [$\sqrt{3} \times \sqrt{3}$] superlattice. NMR analysis of the low doping levels, which clearly shows the formation of Ni^{2+}–Mn^{4+} pairs and some tendency for larger cluster formation, is clearly consistent with this model of strong Ni–Mn ordering disrupted by the Co^{3+} ions. A schematic of this ordering is shown in Figure 17.

Consequences of Cation Ordering for the Electrochemical Behavior. Figure 18 shows the electrochemical profiles and the corresponding derivatives (dx_0/dV) for representative members of the $Li[Ni_xMn_xCo_{(1-2x)}]O_2$ series tested as electrodes in a lithium battery. A shoulder that extends from ca. 3.6 to 3.8 V (left dashed line) is observed in the voltage profile (also see the small peak in the derivative plot) in the initial stages of deintercalation for $0.01 \leq x \leq 0.15$. The amount of extracted lithium correlates with the Ni content, and as a consequence, this process was previously ascribed to the oxidation of nickel from Ni^{2+} to Ni^{4+}.[12] A second process is seen, again for $0.01 \leq x \leq 0.15$, at 3.9 V. The voltage value corresponds to the insulator-to-metal transition of $LiCoO_2$, which has been reported to result in a biphasic region (from approximately $x_0 = 0.95$–0.75) for the undoped material,[43,44] consistent with the presence of a voltage *plateau* in the profile (and a corresponding sharp peak

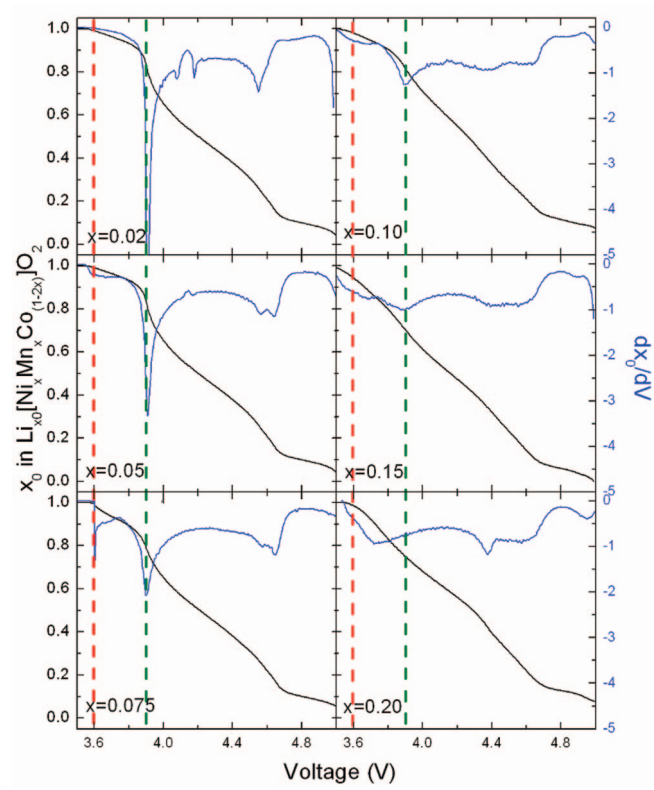

Figure 18. Plot of the voltage versus Li content (x_0 in $Li_{x_0}[Ni_xMn_xCo_{(1-2x)}]O_2$) (black lines) and derivative dx_0/dV (blue lines) of a $Li[Ni_xMn_xCo_{(1-2x)}]O_2$ ($x = 0.02$–0.20) electrode charged against lithium metal at a C/50 rate.

in the derivative). The higher voltage (4 V and onward) processes, noticeable only at low Ni and Mn contents, are associated with a series of phase transitions that occur in $LiCoO_2$ upon removal of 50% or more of the lithium ions.[43,44] The fact that these transitions also take place in samples that contain Ni and Mn indicates that, especially at low contents of these ions, the sample has a considerable $LiCoO_2$-like character. In all of the cases, almost complete removal of the lithium ions from the compound can be achieved at 5 V.

Noticeable changes in the electrochemical profile are seen as Ni doping increases. The most significant is the gradual broadening, and then disappearance when $x = 0.20$, of the peak in the derivative associated with the 3.9 V *plateau*. This can be ascribed to a change in the mechanism of lithium deintercalation, which is no longer two-phase. Instead of showing the 3.9 V *plateau*, when $x \geq 0.20$, the voltage increases gradually with decreasing lithium content to around 4.2 V. This is now associated with a broad peak at around 3.7 V in the derivative curve, because of a single-phase process that results in the extraction of 50% of the lithium. After this reaction, a new process centered around 4.4 V, followed by a gradual increase of the voltage to 4.7 V, accounting for additional 40% of extracted lithium, is observed.

(43) van der Ven, A.; Aydinol, M. K.; Ceder, G. *J. Electrochem. Soc.* **1998**, *145* (6), 2149–2155.
(44) Morcrette, M.; Chabre, Y.; Vaughan, G.; Amatucci, G.; Leriche, J.-B.; Patous, S.; Masquelier, C.; Tarascon, J.-M. *Electrochim. Acta* **2002**, *47*, 3137–3149.
(45) Sears, V. F. *Neutron News* **1992**, *3*, 26.
(46) Welberry, T. R. *Rep. Prog. Phys.* **1985**, *48*, 1543.

These changes in the electrochemical behavior of the samples are strongly correlated with our observations, by ^{6}Li MAS NMR, of the changes in the local structure of the compounds. With increasing Ni and Mn contents, the gradual loss of intensity of the resonance at 0 ppm, resulting from the presence of Li$(Co_6)^{1st}(Co_6)^{2nd}$ local environments, can be associated with the loss of Co-rich domains and is correlated with the gradual broadening and then loss of the peak ascribed to the insulator-to-metal transition seen in the electrochemical profiles. This loss of contact between cobalt ions is likely to interrupt the cooperative effect required for an insulator-to-metallic transition. Once there are no longer any isolated Co^{3+} clusters, a change in the mechanism of the lithium deintercalation is observed. *In situ* XRD and *ex situ* NMR experiments are in progress to provide further insights into the changes in the behavior of compounds in the Li[$Ni_xMn_xCo_{(1-2x)}$]O_2 ($0.01 \leq x \leq 1/3$) series upon oxidation and to fully characterize all of the electrochemical processes.

Conclusions

Several members of the Li[$Ni_xMn_xCo_{(1-2x)}$]O_2 ($0.01 \leq x \leq 1/3$) series, isostructural with layered $LiCoO_2$ (space group $R\bar{3}m$, number 166), were synthesized. The XANES measurements show that these compounds contain Ni^{2+}, Mn^{4+}, and Co^{3+} ions. The ^{6}Li MAS NMR spectra of the compounds show some common features. Several well-resolved resonances can be observed in the compounds with low Ni/Mn contents, and when the amount of Ni and Mn increases, these resonances start to merge and finally form a broad resonance. The chemical environments of the resonances in the spectra for low Ni/Mn contents ($x \leq 0.10$) were assigned using prior NMR analyses of paramagnetic materials to different arrangements of transition-metal cations in the first and second coordination shells.

In the very dilute sample, ^{6}Li[$Ni_{0.02}Mn_{0.02}Co_{0.96}$]$O_2$, analysis of the ^{6}Li MAS NMR spectra indicates the formation of Ni^{2+}/Mn^{4+} clusters in the predominantly Co^{3+}-containing TM layers. Moreover, it has been found that the oxidation state of Ni in this high Co content sample is highly dependent upon the starting Li/transition metal ratio, with the NMR spectrum of a sample containing 5% Li excess showing peaks associated with the presence of Ni^{3+}. Neutron PDF analysis of Li[$Ni_{1/3}Mn_{1/3}Co_{1/3}$]O_2 shows a nonrandom distribution of Ni and Mn cations in the TM layers, with Ni closer to Mn in the first coordination shell (resembling the [$\sqrt{3} \times \sqrt{3}$] R30°-type superlattice structure model) but a more random distribution of Co. The ^{6}Li NMR spectrum of this compound and an analysis of the intensity of the resonance assigned to Co^{3+}-rich regions, for the whole Li[$Ni_xMn_xCo_{(1-2x)}$]O_2 series, is also consistent with the PDF results, indicating a nonrandom distribution of transition-metal cations in the TM layers. The local ordering was correlated with variations in the mechanism of lithium intercalation with increased Ni/Mn content. The most significant change was the conversion of the two-phase reaction ascribed to the insulator-to-metal transition, as reported for stoichiometric $LiCoO_2$, first into a broader process and then the total disappearance of this process for $x \geq 0.20$. The decrease in the concentration of Co-rich clusters in the pristine materials as seen by NMR is strongly correlated with these changes.

These results suggest that Ni and Mn show a strong tendency for clustering in the TM layers all along the Li[$Ni_xMn_xCo_{(1-2x)}$]O_2 ($0.01 \leq x \leq 1/3$) series. The results provide further insight into the structural features of these compounds, which are currently of high interest as positive electrodes in lithium-ion batteries.

Acknowledgment. This work was supported by the Assistant Secretary for Energy Efficiency and Renewable Energy, Office of FreedomCAR and Vehicle Technologies of the U.S. DOE, under contract number DE-AC03-76SF00098, via subcontract numbers 6517748 and 6517749, with the Lawrence Berkeley National Laboratory. We also acknowledge support from the Intense Pulsed Neutron Source at Argonne National Laboratory. This facility is funded by the U.S. DOE under contract number W-31-109-ENG-38. Use of the NSLS, Brookhaven National Laboratory, was supported by the U.S. DOE, Office of BES, under contract number DE-AC02-98CH10886. We are grateful for the assistance given to us at IPNS from James Richardson and Evan Maxey. J.C. thanks the Generalitat de Catalunya (Spain) for funding, via a Beatriu de Pinós fellowship. We thank Kisuk Kang (MIT) and Meng Jiang (Stony Brook University) for kindly supplying the samples of $Li_{0.9}[Ni_{0.45}Ti_{0.55}]O_2$ and Li_2MnO_3, respectively.

Supporting Information Available: Refinement results of the cell parameter for all of the samples, from XRD data. This material is available free of charge via the Internet at http://pubs.acs.org.

CM702241A